Nanosensors for In-vivo Opto-Chemical Imaging of Sodium Ions

ZHANG, WULIANG

KOPELMAN GROUP, UNIVERSITY OF MICHIGAN

Nanosensors for *In-vivo* Opto-Chemical Imaging of Sodium Ions

By

Wuliang Zhang

ABSTRACT

Sodium ions are very important in cellular biochemical reactions and metabolism; they participate in the intracellular protein synthesis and carbohydrate metabolism.[1,2] Given the importance of sodium ions, probes that are able to visualize the physiological Na^+ behavior are necessary. To achieve this goal, sodium ion-selective optical nanosensors were prepared for *in-vivo* photoacoustic imaging. They were based on the incorporation of Sodium Ionophore III and an indicator dye, Chromoionohore I.[3-7] They were embedded in Pluronic micelles with another layer of polybutyl methacrylate nanoparticles within the micelles. The polybutyl methacrylate nanoparticles were formed via free-radical polymerization. The diameter of the sensors in Tris buffer was around 40 nm. The sodium sensors were characterized by UV-Visible spectroscopy. Photoacoustic spectroscopy will also be applied to calibrate the sodium sensors. Notably, photo-acoustic application uses the same principles as that of UV-VIS spectroscopy,[4] but is not limited by photon tissue penetration.[5]

TABLE OF CONTENTS

INTRODUCTION

Sodium is one of the major ions in biological systems, together with other metal ions such as K^+, Mg^{2+}, Ca^{2+}, etc. Na^+ is involved with regulating the concentration of other ions, such as Ca^{2+} and Cl^-, across the cell membrane, which is responsible for cell signaling.[1,2] The cellular Na^+ has its leading roles in transmembrane transport and cell signaling. The potential energy stored in the Na^+ gradient is commonly coupled with the uptake of nutrients, e.g. amino acids, sugars, and transmitters, into cells against their concentration gradients.[1] In addition, it also facilitates substrate binding by lowering the energetic barrier; in particular, extracellular enzymes generally use Na^+.[1,2] Given the importance of sodium ions, real-time monitoring of the sodium ion concentration in body is of great research interest.[3-7]

Traditionally, the concentration of a certain ion is measured by an ion-selective electrode. However, this is far from ideal for *in vivo* studies, because it is invasive and a real-time monitoring is impossible.[4] On the other hand, optical probes encapsulated by biologically compatible embedding, called nano-PEBBLES, can achieve minimal chemical interference.[3-7] Optical nanosensors use the same highly selective ionophores as do ion-selective electrodes; here the surface of the nanosensors acts as the ion-selective membrane applied in electrodes.[6] These sensors while showing high selectivity and sensitivity,[3-5] also allow real-time imaging of the of the Na^+ concentration and its fluctuation.[3] Ion-selective indicators, whose absorption and emission reflect the local concentration of the ion, have been used

for optical sensing.[7] For example, Sodium Green is used for Na^+ sensing[22]. Although these indicators are widely used, they suffer from some drawbacks such as cytotoxicity, heavy metal interference, and dye leakage.[21] In comparison, nanosensors incorporating a certain type of pH indicator (chromoionophore) is universal to sensing of any ion, which only varied by the type of ionophore.[21]

The Kopelman group was the first one to devise a nanoparticle-based real-time optical ion sensor.[3,4] The general formulation of ion-selective optodes contains a matrix of plasticized polymer, a pH-responsive dye (Chromoionophore-1), an ionophore, and an ionic salt facilitating ion exchange within the sensor's hydrophobic core.[3-5,7] In the case of sodium ion sensing, the ionophore selectively carries a sodium ion into the sensor, followed by the deprotonation of the Chromoionophore 1, in order to maintain the charge neutrality in the hydrophobic core of the nanosensor. The change in the absorption spectrum of the Chromoionophore-1 reflects this protonation change.[3-5,7]

To incorporate the hydrophobic pH dye and ionophore into a biocompatible matrix, a polymer with amphiphilicity is required. Amphiphilic block copolymers, when placed in aqueous phase, can form core-shell nano-sized aggregates, which can solubilize poorly soluble drugs and thus improve their bioavailability. The same principle can be applied to lipophilic sensing components. Pluronic® is a series of triblock copolymers of poly (ethylene oxide) (PEO) and poly (propylene oxide) (PPO) with the structure PEO-PPO-PEO. They can self-assemble into micelles, which are composed of EO as the hydrophilic outer shell, and PO as a hydrophobic inner core. Micelles

composed of two or more different copolymers can have synergistic properties, such as increased micelle stability. It was proposed that by mixing Pluronic P123, a copolymer with large hydrophobic (PPO) group, and Pluronic F68, one with large hydrophilic (PEO) group, the stability and solubility of the loaded drug can be improved.[19]

Our group has previously reported on a variety of ion sensing nanoparticles for single cell analyses, all based on fluorescence imaging.[4] However, in vivo monitoring of ion using fluorescence imaging has been a challenge due to limitations of the penetration depth by most biological tissues.[8-10] To overcome the penetration depth limit, the photoacoustic imaging (PAI) method can be applied. PAI is based on the absorption change of the indicator dye, as the degree of protonation changes. The absorbed photons are mostly dissipated as heat, and are detected as ultrasound signals, as the heat generated pressure wave propagates through the surrounding area (figure 1).[7,8] This PAI method can thus be thought of as a miniaturized UV-VIS spectrophotometer put inside the body. Because the ultrasound scattering in tissue is two to three orders of magnitude weaker than optical scattering, a higher spatial resolution can be realized.[9] In recent years, PAI has been widely applied in biomedical fields, including cancer,[10-12] brain vasculature and function,[13-15] cardiovascular,[16] and tissue engineering scaffolds,[17,18] prompting translational advances in clinical PAI. However, up to now, PAI has been limited to structural imaging, based on spatial laser scanning. The above approach of chemical PAI, or functional PAI (f-PAI), where the laser is also scanned spectrally, was originated by the Kopelman group only recently.[8,23,24]
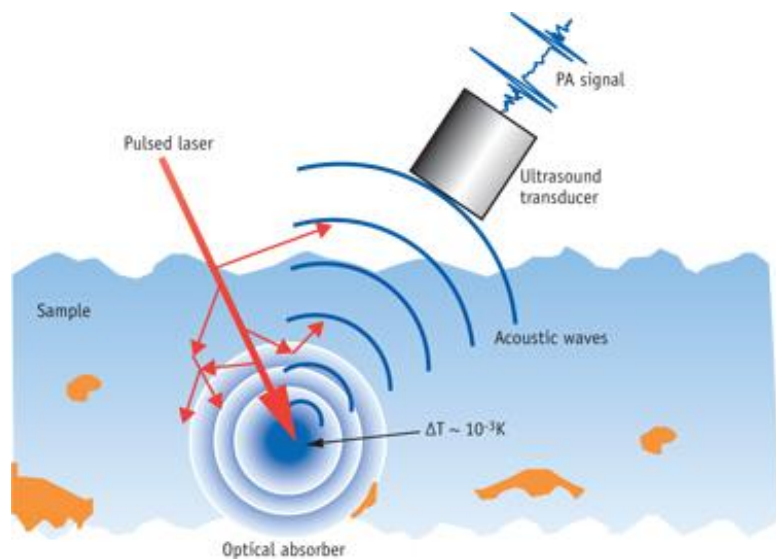
Figure 2. Photoacoustic signal generation and detection. Curtsey of Jie et al., 2014.[20]

In this work, the Pluronic P123/F68 copolymer matrix self-assembled into micelles in aqueous phase. Besides the three sensing components (the sodium ionophore, the chromoionophore, and the ionic salt), a monomer, plasticizer, and a crosslinker were also added to the copolymer matrix. Polymerization led to the formation of a second layer of polymer network within the Pluronic micelle to further stabilize the sensor. Absorption data collected via UV-Vis illustrated high sensitivity and selectivity to sodium ions.

EXPERIMENTAL METHODS

General Considerations. Unless otherwise stated, chemicals were used as purchased without further operation. UV-Vis data were collected at the University of Michigan Department of Chemistry technical services.

Materials. Pluronic P123, Pluronic F68, dichloromethane (DCM), bis(2-ethylhexyl) sebacate (DOS), 1,6-hexanediol dimethacrylate (HDMA), butyl methacrylate (BMA), 3-octadecanolymino-7-(diethylamino)-1,2-benzophenoxazine (chromoionophore 1, or CHI1), sodium tetrakis [3,5-bis(trifluoromethyl) phenyl] borate (NaTFPB), 4-tert-Butylcalix[4]arene-tetraacetic acid tetraethyl ester (sodium ionophore X, or NaI10), N,N,N',N'-tetramethylethane-1,2-diamine (TEMED), Ammonium persulfate (APS) and 2-amino-2-hydroxymethyl-propane-1,3-diol (Tris).

Preparation of Na$^+$-Selective Micelles. 116 mg of Pluronic P123, 84mg of Pluronic F68, 5 μL of HDMA, 5 μL of BMA, 14 μL of DOS, 0.925 mg of CHI1, 4.5 mg of NaTFPB, and 4.75 mg of NaI10 were dissolved in 4 mL of DCM to form a homogeneous solution. The solvent was removed under reduced pressure by rotary vacuum evaporation to obtain a purple thin film. The resulted film was further dried under nitrogen gas flow for thirty minutes to remove any residual. After that, the film was hydrated in 5 mL of Millipore water. An Ultrasonic instrument was employed to disperse the film via ultrasound and form a homogeneous purple micellar suspension. The resulting solution was filtered through a 0.45 μm syringe filter (Millipore).

Polymerization of Na⁺-Selective Micelles. The micellar suspension was transferred to a conical centrifuge tube with a 100kDa filter unit and centrifuged (4000G, 20 min) to remove any excess Pluronic copolymer. To a 50 mL round bottom flask equipped with a Teflon stir bar, the purple micellar solution was added and the flask was sealed. The solution was purged under Argon gas for five minutes before 10µL of TEMED and APS (10% w/w) were injected to initialize the radical polymerization. The reaction was allowed for two hours under Argon gas flow before it was quenched by exposed to air. The red reaction mixture was then transferred to a conical centrifuge tube with a 100kDa filter unit and centrifuged at 4000G for 40 minutes. After that, the yielded red solution was washed with 10 mM Tris buffer (pH adjusted to 7.4) for at least five times via centrifugation (4000G, 40 minutes each cycle), which then yielded dark blue solution. Final products were stored at 4ºC.

Na⁺-Selective Nanosensor Size and Zeta Potential Measurements. Hydrodynamic diameters and zeta potential were measured using Delsa™ Nano C particle size analyzer by Beckman Coulter Instruments Corporation. All measurements were taken on the diluted nanosensor solution in 10mM Tris buffer, pH 7.4 so that the detector had optimum signal intensity. The detector measured scattered light at 638 nm, and calculated the effective diameter based on the intensity of scattered light. Zeta potentials were measured though electrophoretic light scattering.

Response to Sodium Ions. The nanosensor was calibrated for its absorption response to sodium ion concentration change in 10mM Tris buffer solution at pH 7.4. For each calibration point, the micelle solution was mixed with standard NaCl

solutions so that the final NaCl concentrations were from 0-500 mM and a total of 12 calibration points were retrieved. Each concentration was performed in triplicate from three different sets of nanosensors. The absorption intensities of CHI1 were measured with Shimadzu UV1601. The absorption ratio was calculated as

$$R = \frac{664 \, nm \, absorption}{538 \, nm \, absorption}.$$

Test the Selectivity of the Na+-Nanosensor. The selectivity was tested in two methods. In the first method, similar to the test of the response to sodium ions, the nanosensor solution was mixed with KCl and $CaCl_2$-Tris solution of various cation concentration. UV-Vis spectra of these nanosensor-K^+/Ca^{2+} solution were obtained and the ratiometric analysis was based on the plot of the absorption ratio R vs. log (cation concentration) (mM). In the second method, since potassium is the primary interference of the sodium ion sensing, the selectivity was examined by measuring the nanosensor absorption response to 0, 0.05, 0.25, 0.5, 2.5, 5, 10, 25, 50, 75, 100, and 250 mM of sodium ions in static concentrations of potassium background. The background potassium concentration for each calibration curve was set to 0, 4, and 100 mM, respectively; the latter two potassium ion concentration is typical in extracellular and intracellular environment,[1] respectively. Absorption intensities of CHI1 were measured in a disposable cuvette (with a path length of 1 cm) and the absorption ratio was calculated as $R = \frac{664 \, nm \, absorption}{538 \, nm \, absorption}$, at the potassium background of 4 and 100 mM. At static concentrations of sodium background (10 and 150 mM, respectively), the response of the nanosensors to potassium ions was examined. The absorption ratio was calculated as $R' = \frac{654 \, nm \, absorption}{528 \, nm \, absorption}$, for the ratiometric analysis.

Statistical analysis. All experiments were performed in triplicate and analyzed on Excel. Values are represented numerically as mean± standard deviation, and graphical representations contain error bars for the standard deviation values. Significance was designed at 95% confidence level ($\alpha=0.05$), determined by the ANOVA test on Excel.

RESULTS AND DISCUSSION

Effect of Radical Polymerization

Micelles were formed through sonicating the thin film in water. DOS, as used in previous studies,[5,7] acts as a plasticizer to prevent the micelle-coated nanosensors from aggregating. Different from previous studies that directly used micelles as the nanosensors, HDMA and BMA were loaded into the micelle to allow radical polymerization (scheme 1), leading to smaller micelle size and narrower size distribution.
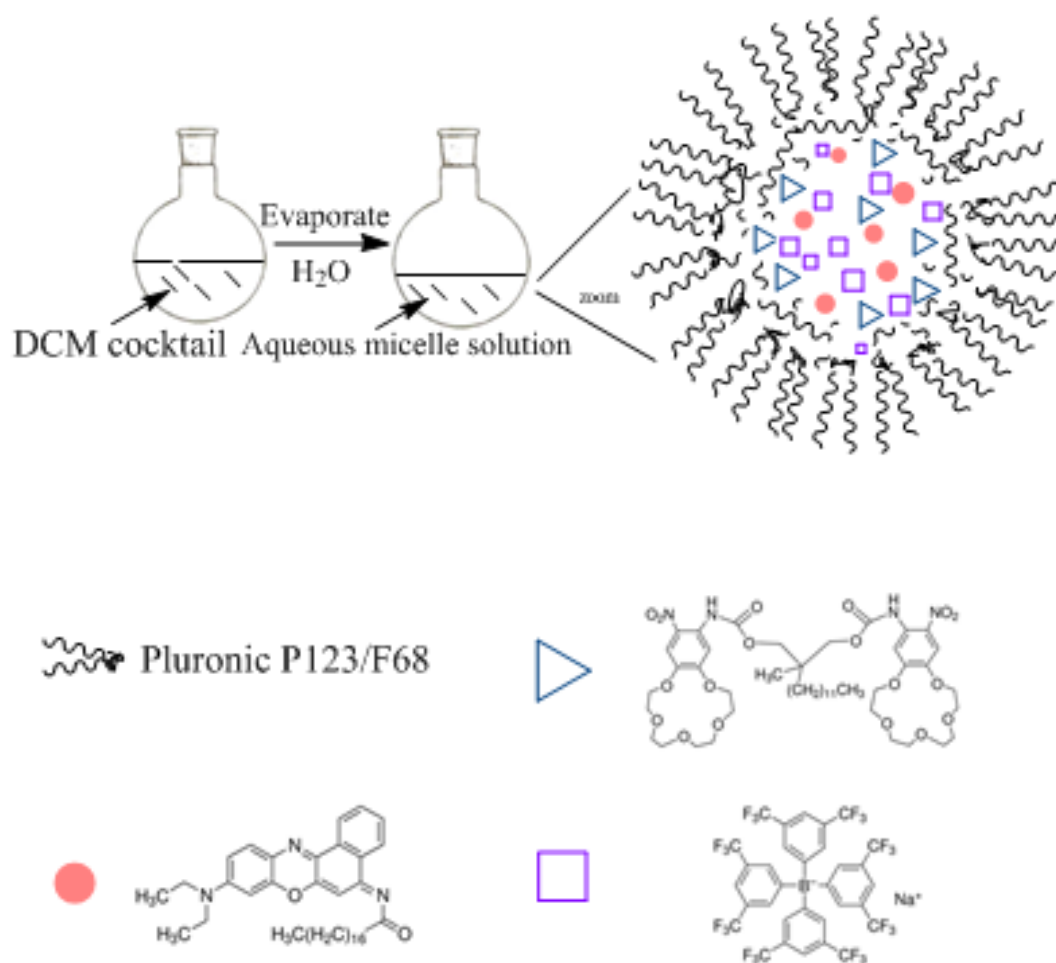
Scheme 1. Preparation schematic of the sodium ion-selective nanosensor.

Based on preliminary studies, the size of the micelle formed before polymerization was 105 nm, with a PDI 0.426; the diameter was down to 62 nm after polymerization, with a PDI 0.3, where PDI indicated the variation of the size distribution. It indicated that polymerization not only reduced the average size of nanosensors, but also improved the monodispersity.

Furthermore, to ensure the sensitivity of the nanosensors, the core of the nanosensor should be maintained highly hydrophobic to avoid leakage of any sensing component, so that interfering ions will not easily enter. Addition of the hydrophobic compounds, HDMA and BMA, is conducive to maintain the hydrophobicity of the micelle core.

Characterization of the sodium ion sensors

The hydrodynamic diameters of the polymerized nanosensors were obtained from the Dynamic Light Scattering (DLS). Zeta potential was measured through applied electric field, in which particles migrated and thus electrophoretic mobility and zeta potential were obtained. The size distribution of DLS suggests a unimodal distribution centered around 40 nm (figure 2). The nanosensor was in a Tris buffer solution at the physiological pH 7.4. Although PBS buffer is commonly used for simulation of the physiological environment, it contains Na^+ and K^+ that might interfere with the calibration of the nanosensors. Therefore, a non-ion-contained Tris buffer was chosen for this study.
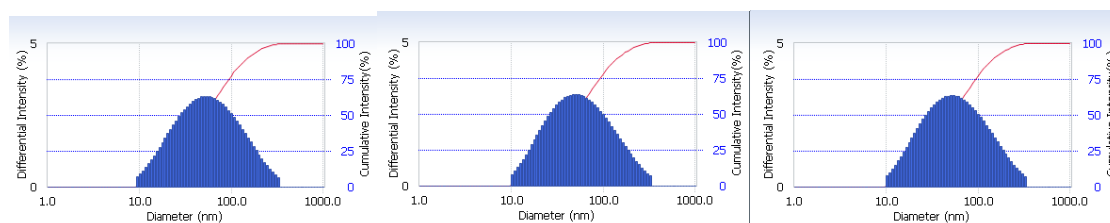

Figure 3. Size distribution of sodium ion-selective nanosensor measured by DLS.

The average hydrodynamic diameter of the sodium nanosensors is 42.7±3.3nm, with average PDI 0.34±0.03. The average zeta potential is -58.6±20.9 mV. The difference among average size and PDI across the triplicates are not statistically significant at 95% confidence level, based on the ANOVA test. The large standard deviation in the zeta potential measurement could be caused by instrumental drift or the deviation of Tris buffer from the instrument default solvent (water).

Response to Change of the Na⁺ concentration

Sensing of sodium ion is achieved by the deprotonation of chromoionophore I once Na⁺ binds to NaI 10 and enters the micelle, causing absorption spectral change of the chromoionophore (scheme 2).
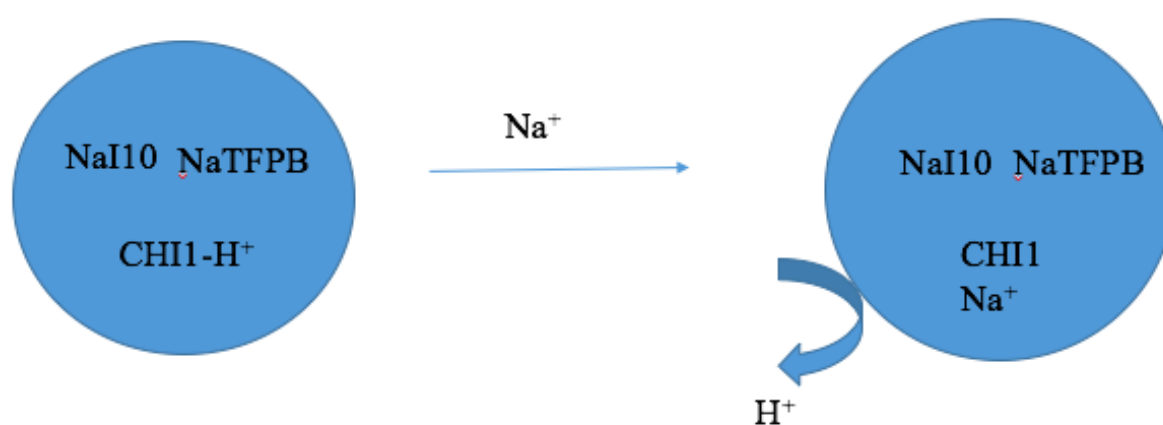
NaI10= Sodium ionophore X
NaTFPB= Sodium tetrakis[3,5-bis(trifluoromethyl)phenyl]borate
CHI1= Chromoionophore I

Scheme 2. Deprotonation of the chromoionophore-I with the introduction of Na⁺ into the Na⁺-selective nanosensor.

NaCl solution was added to each nanosensor solution with a concentration ranging from 0-500 mM. The color gradient can be easily visualized (figure 3).

Figure 4. Color gradient of sodium ion sensors in [Na$^+$] of 0, 0.1, 0.5, 1, 5, 10, 20, 50, 100, 150, 200, and 500 mM.

The Na$^+$ response of the nanosensors in absorbance mode is shown in figure 4. CHI1 is a ratiometric dye and it shows a visible response to Na$^+$ with an isosbestic point at around 572 nm.
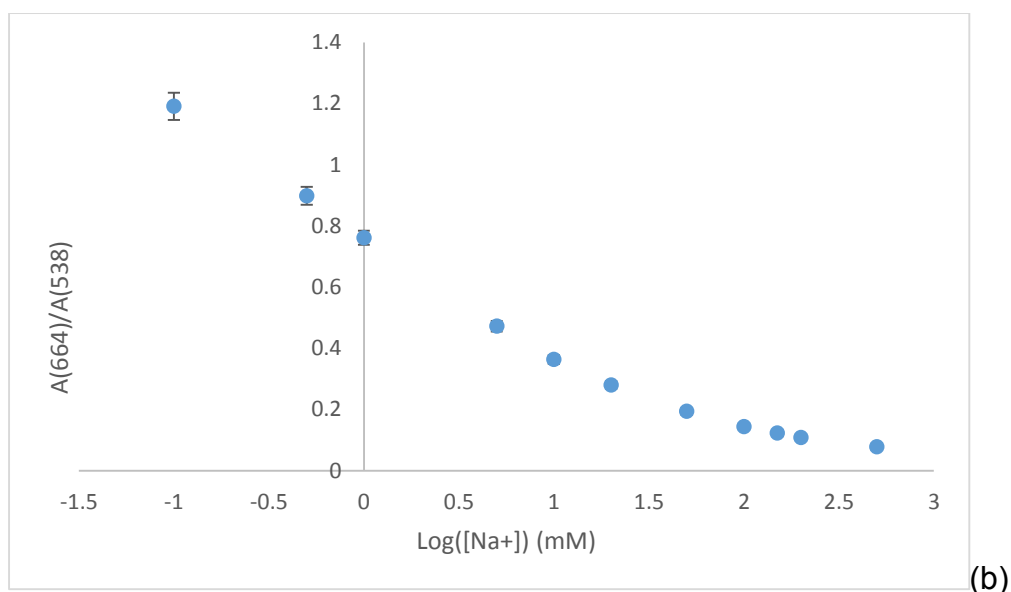

(a)

(b)
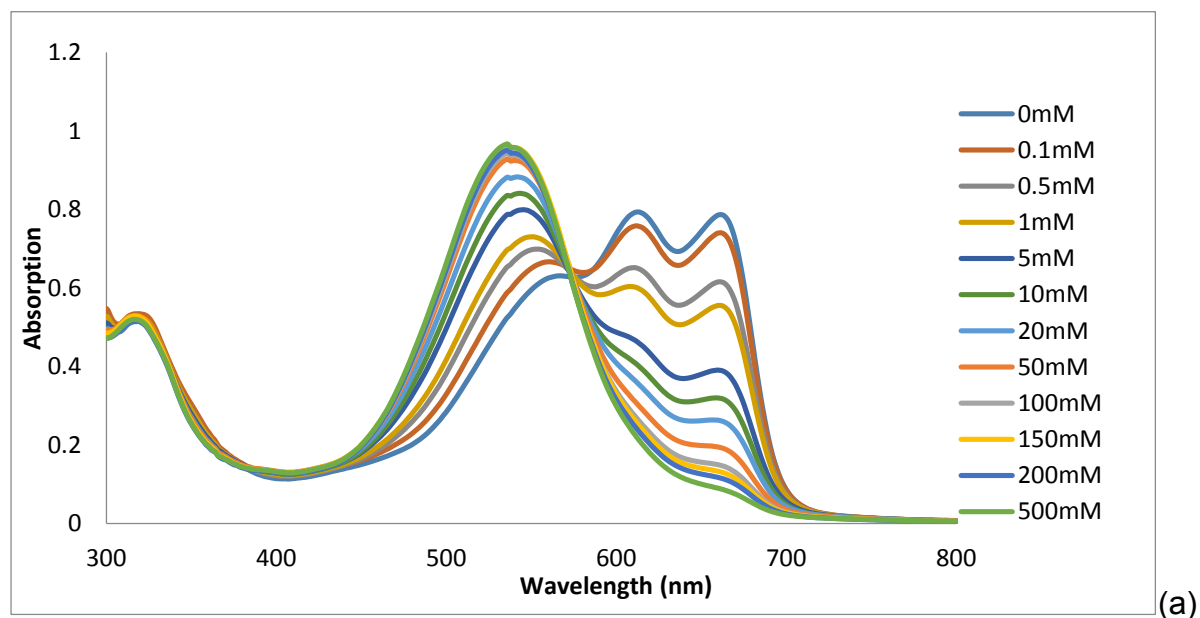
Figure 5. Na$^+$ response of Pluronic F68/P123-based nanosensors containing CHI1, NaTFPB, and NaI10 in 10mM Tris buffer. (a) Absorption spectra at different Na$^+$ concentration. (b) Calibration curve using absorbance ratio at 664 and 538 nm.

The dynamic range covers 0-500 mM, so this type of sensor is applicable to sodium ion concentration measurements in physiological environment (where [Na$^+$] is typically below 200 mM). With increased sodium concentrations, the absorption peak at 538 nm increases in intensity (figure 4a) and the absorption at 664 nm decreases in intensity as CHI1 becomes increasingly deprotonated. The ratiometric plot of the absorption ratio at 664 and 538 nm as a function of log ([Na$^+$]) (in mM) is shown in figure 4b. The absorption ratio was well resolved even between the [Na$^+$] of 0 and 0.1 mM, indicating high sensitivity of the nanosensors.

Na$^+$ selectivity of the nanosensors

It is possible that the deprotonation of CHI1 could be caused by the transfer of ions other than Na$^+$, which might interfere with the correct measurement of Na$^+$

15

concentration. Therefore, one requires the optode response to be sodium-ion-selective. The response of the nanosensor solution was evaluated in comparison to K^+ and Ca^{2+} ions. Due to the low physiological concentration of Ca^{2+} (typically lower than 2mM)[7], the interfering Ca^{2+} was tested up to 5 mM. As shown in figure 5, the nanosensor is highly selective for Na^+ over K^+ and Ca^{2+}.
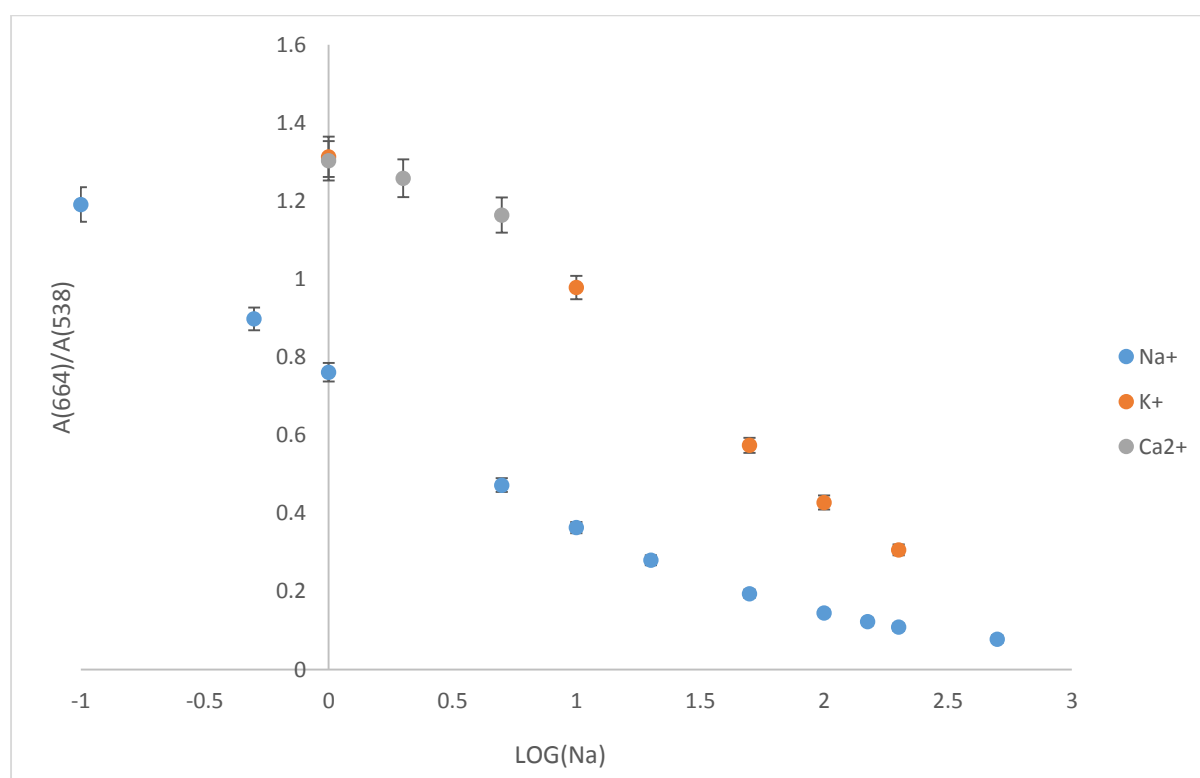

Figure 6. Selectivity of the Na^+-selective nanosensors measured in 10mM of pH 7.4 Tris-HCl buffer solution in absorption mode. Data represented as mean values with error bars for standard deviation.

The higher absorption ratios of the K^+ and Ca^{2+} responses, compared to that of Na^+, indicate that under the same concentration, K^+ and Ca^{2+} caused smaller spectral shift of the CHI 1 from its protonated state. The selectivity of Na^+ over K^+ is at least one order of magnitude higher, indicating that without the presence of any other ion, K^+

will not contribute much to the absorption change of CHI 1. The linear dynamic range of the sodium response, without the presence of any other ion, roughly covers a $[Na^+]$ from 0.1 to 100 mM, with an R^2 around 0.99. At higher Na^+ concentrations, the nanosensor response began to deviate from linearity, indicating that the sodium ionophore started to saturate.

Na⁺ response at a constant potassium background

Na⁺ response at a constant potassium background

Potassium ion is the major interference to sodium ion sensing. To mimic the biological system, the response to sodium ions of the nanosensors were measured in the presence of two static potassium backgrounds, of 4 and 100 mM, which are typical extracellular and intracellular potassium ion concentration, respectively. At the constant potassium ion background, the nanosensors showed response to Na^+ at both low and high $[K^+]$ (figures 6 and 7).
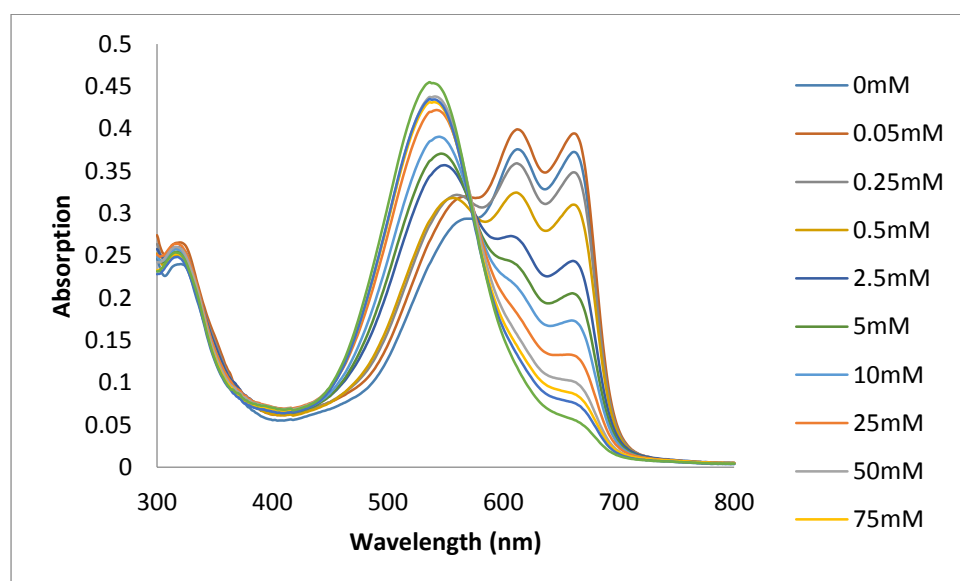

Figure 7. Absorption spectrum of Na^+ response at a constant K^+ background of 4 mM.
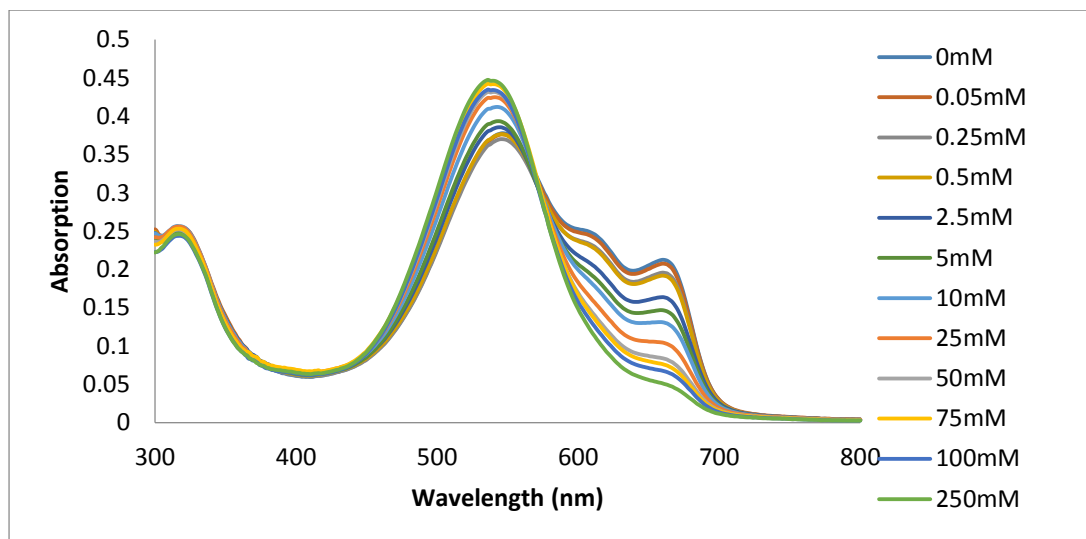
Figure 8. Absorption spectrum of Na$^+$ response in a constant K$^+$ background of 100 mM.

The overlaid calibration curves of the Na$^+$ response at potassium backgrounds of 0, 4, and 100 mM can be seen in figure 8. Under all three of the static potassium backgrounds, it appears that all the sodium ion concentrations tested are covered by the dynamic range (figures 8 and A3).
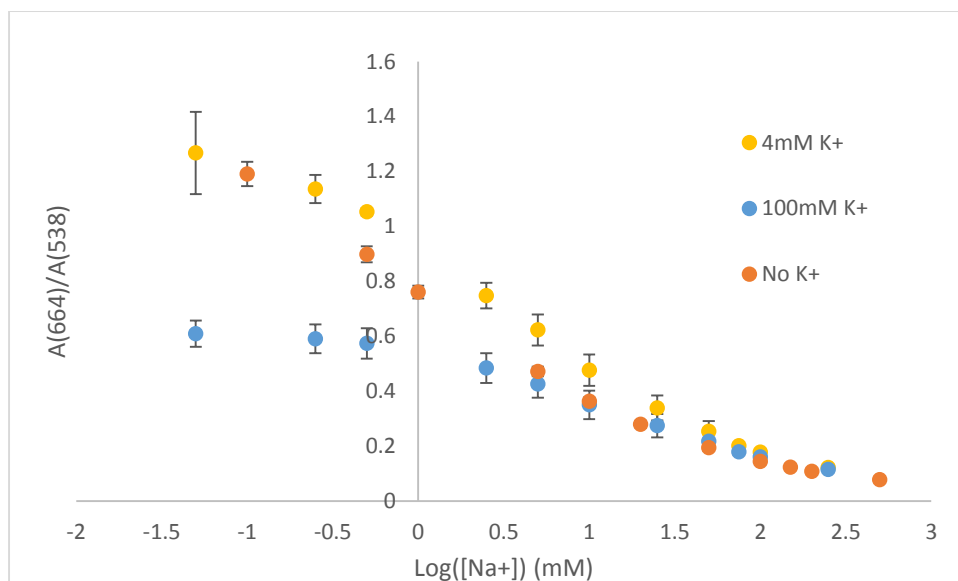
Figure 9. Calibration curve of the Na$^+$ response of the nanosensors in a constant K$^+$ background of 0 (orange), 4 (yellow), and 100 mM (blue). Data represented as mean values with error bars for standard deviation.

The difference in variances among triplicate measurements in all three sets of Na$^+$ response data are not statistically significant at 95% confidence level, based on the ANOVA test. It is observed that at the 100 mM K$^+$ background, the absorption change is minuscule when [Na$^+$] changes from 0.05 to 0.25 mM. Notably, the higher the concentration of the potassium background is, the less sensitive the nanosensors are to sodium ions, and the less distinctively the absorption ratio changes. The response to sodium ion concentration is roughly one order of magnitude greater at the background of 4 mM of K$^+$ than at 100 mM of K$^+$. However, under the 100 mM K$^+$ background, when [Na$^+$] is greater than 5 mM, the Na$^+$ response became similar to the response without any potassium background. Therefore, in biological conditions, where sharp changes in the sodium ion concentration occur, e.g. with cell signaling,[2] these nanosensors can detect [Na$^+$] changes under both high and low potassium concentration background.

K+ response at a constant sodium background

To further prove that the change of the absorption ratio caused by potassium ion is not as significant as for sodium ions, the K+ response was tested at a constant sodium bakcground of 10 and 150 mM, respectively. These two sodium background concentration were selected to mimic the physiological conditions.

The overlaid calibration curve of the K+ response at static sodium background of 10 and 150 mM, and Na+ response at a static potassium background of 100 mM, can be viewed in figure 9. At 150 mM of Na+ background, the nanosensor seemed to be irresponsive to the change of K+ concentration, where the absorption ratio barely changed when [K+] increased from 1 to 200 mM. At a 10 mM of sodium ion background, the change of the absorption ratio caused by the change of the K+ concentration from 0-200 mM is approximately the same as the [Na+] change from 0-10 mM at a static 100mM of potassium background. Therefore, even at low sodium concentration backgrounds (i.e. 10 mM of [Na+]), the absorption ratiometric change caused by potassium ions is at least 20 times less significant than that of sodium ions, which further corroborates the high selectivity of the nanosensors to sodium over potassium ions.
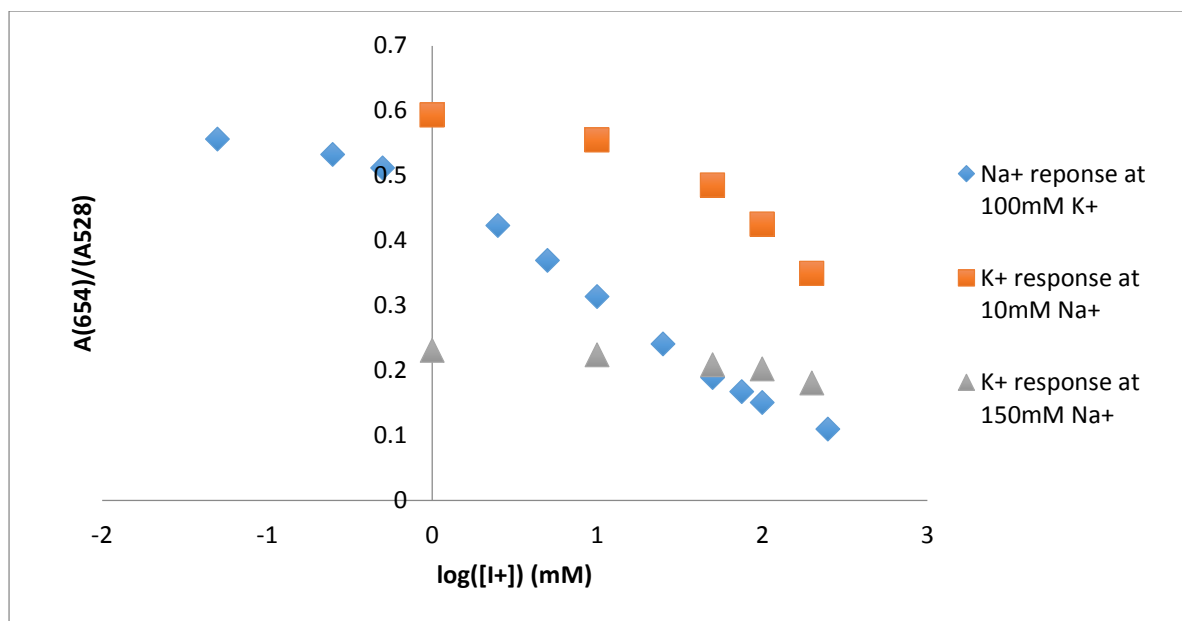
Figure 10. Calibration curve of the Na$^+$ response of the nanosensors in a constant 100 mM K$^+$ background (blue), and the K$^+$ response in a constant Na$^+$ background of 10 mM (orange), and 150 mM (grey). I$^+$ could be Na$^+$ or K$^+$.

CONCLUSIONS

A sodium ion-selective nanosensor for biological sodium ion concentration imaging is fabricated as a sodium ionophore-based ion-selective optode. The incorporation of the sodium ionophore, ionic salt, and chromoionophore renders the selectivity and sensitivity to sodium ions. Radical polymerization gives smaller and more monodisperse size distribution of the nanosensors. The zeta potential measurement indicates a negative surface charge. The results from UV-Vis measurements indicate high sensitivity and selectivity of the nanosensors in a physiological range of sodium ion concentration. The sensitivity to the variation of the biological sodium ion concentration remains valid regardless of the background concentration of

potassium ions. Moreover, the nanosensor is at least 20 times less responsive to [K$^+$], even at low sodium ion concentration background. Therefore, the interference of K$^+$ is not a significant issue to the sodium ion sensing using the nanosensors fabricated in this study. These nanosensors could be applied to image brain activities, where neuron firing induces great influx/ reflux of sodium ions. In addition, the design of the nanosensor is a universal one. It could be used for any ion sensing, by just varying the ionophore. Using the same rationale, potassium and calcium ion sensors have also been developed in our lab.

FUTURE WORK

The nanosensors will be calibrated via photoacoustic imaging. After that, in vitro sodium ion measurement will be tested using photoacoustic imaging. In addition, the the nanosensors will be functionalized by attaching amine groups to the surface, and after that, a targeting moiety will be attached to designate a cellular destination to the nanosensors.

REFERENCES

(1) Clausen, Michael Jakob Voldsgaard; Poulsen, Hanne. "Chapter 3 Sodium/Potassium Homeostasis in the Cell". In Banci, Lucia (Ed.). Metallomics and the Cell. Metal Ions in Life Sciences 12. Springer **2013**.

(2) Sigel, A.; Sigel, H.; Sigel, R.; Pohl, H.; Wheeler, J.; Murray, E. Metal Ions in Life Sciences. *Met Ions Life Sci* **2013**.

(3) Brasuel, M.; Kopelman, R.; Miller, T.; Tjalkens, R.; Philbert, M. Fluorescent Nanosensors for Intracellular Chemical Analysis: Decyl Methacrylate Liquid Polymer Matrix and Ion-Exchange-Based Potassium PEBBLE Sensors with Real-Time Application to Viable Rat C6 Glioma Cells. *Anal. Chem.* **2001**, *73*, 22212228.

 (4) Buck, S.; Xu, H.; Brasuel, M.; Philbert, M.; Kopelman, R. Nanoscale Probes Encapsulated by Biologically Localized Embedding (PEBBLEs) for Ion Sensing and Imaging in Live Cells. *Talanta* **2004**, *63*, 41–59.

(5) Ruckh, T.; Mehta, A.; Dubach, M.; Clark, H. Polymer-Free Optode Nanosensors for Dynamic, Reversible, and Ratiometric Sodium Imaging in the Physiological Range.*Sci. Rep.* **2013**, *3*, 3366.

(6) Bühlmann, P.; Pretsch, E.; Bakker, E. Carrier-Based Ion-Selective Electrodes and Bulk Optodes. 2. Ionophores for Potentiometric and Optical Sensors. *Chem. Rev.* **1998**,*98*, 15931688.

(7) Xie, X.; Zhai, J.; Bakker, E. pH Independent Nano-Optode Sensors Based on Exhaustive Ion-Selective Nanospheres. *Anal. Chem.* **2014**, *86*, 28532856.

(8) Ray, A.; Yoon, H.; Lee, Y.; Kopelman, R.; Wang, X. Sonophoric Nanoprobe Aided pH Measurement in Vivo Using Photoacoustic Spectroscopy. *Analyst* **2013**, *138*, 3126–3130.

(9) Xu, M.; Wang, L. Photoacoustic Imaging in Biomedicine. *Rev. Sci. Instrum.* **2006**, *77*, 041101.

(10) Bayer, C.; Luke, G.; Emelianov, S. Photoacoustic Imaging for Medical Diagnostics. *Acou. Today* **2012**, *8*, 15.

(11) Mallidi S, Luke GP, Emelianov S. Photoacoustic imaging in cancer detection, diagnosis, and treatment guidance. *Trends in Biotechnol*. **2011**, *29*, 213–221.

(12) Laufer J, Johnson P, Zhang E, Treeby B, Cox B, Pedley B, Beard P. In vivo preclinical photoacoustic imaging of tumor vasculature development and therapy. *J Biomed Optics*. **2012**, *17*, 056016–1.

(13) Stein EW, Maslov K, Wang LV. Noninvasive, in vivo imaging of blood-oxygenation dynamics within the mouse brain using photoacoustic microscopy. *J Biomed Optics*. **2009**, *1,* 020502020502.

(14) Laufer J, Zhang E, Raivich G, Beard P. Three-dimensional noninvasive imaging of the vasculature in the mouse brain using a high resolution photoacoustic scanner. *Appl Optics*. **2009**, *48*, D299.

(15) Tsytsarev V, Maslov KI, Yao J, Parameswar AR, Demchenko AV, Wang LV. In vivo imaging of epileptic activity using 2-nbdg, a fluorescent deoxyglucose analog. *J Neurosci Methods*. **2012**, *203*, 136.

(16) Taruttis A, Herzog E, Razansky D, Ntziachristos V. Real-time imaging of cardiovascular dynamics and circulating gold nanorods with multispectral optoacoustic tomography. *Optics Express.* **2010**, *18*, 19592.

(17) Cai X, Paratala BS, Hu S, Sitharaman B, Wang LV. Multiscale photoacoustic microscopy of single-walled carbon nanotube-incorporated tissue engineering scaffolds. *Tissue Engineering Part C Methods.* **2012**, *18*, 310.

(18) Nam SY, Ricles LM, Suggs LJ, Emelianov SY. In vivo ultrasound and photoacoustic monitoring of mesenchymal stem cells labeled with gold nanotracers. *PLoS ONE.* **2012**, *7*, e37267.

(19) Zhao, L.; Du, J.; Duan, Y.; Zang, Y.; Zhang, H.; Yang, C.; Cao, F.; Zhai, G. Curcumin Loaded Mixed Micelles Composed of Pluronic P123 and F68: Preparation, Optimization and in Vitro Characterization. *Colloids and Surfaces B: Biointerfaces* **2012**, *97*, 101108.

(20) Jie, H.; Cheng, J. X. Vibrational Potoacoustic Microscopy: Converting Molecular Vibration to Mechanical for Deep-Tissue Imaging. *BioOptics World* **2014**, *7*, 4.

 (21) Xie, X.; Mistlberger, G.; Bakker, E., Ultrasmall fluorescent ion-exchanging nanospheres containing selective ionophores. *Analytical chemistry* **2013**, *85* (20), 9932-8.

(22) Kim, M. K.; Lim, C. S.; Hong, J. T.; Han, J. H.; Jang, H.-Y.; Kim, H. M.; Cho, B. R. Angew. Chem., Sodium-Ion-Selective Two-Photon Fluorescent Probe for *In Vivo* Imaging. *Int. Ed.* **2010**, 49, 364.

(23) S. Ashkenazi, R. Kopelman, Y.E.L. Koo, T. Horvath and S. Wang, Oxygen sensing for in-vivo imaging by Photoacoustic lifetime probing. *SPIE Proceedings* **2008**, *6856*, 68560D-1-5.

(24) T. Horvath, S. Ashkenazi, R. Kopelman. Ratiometric Photoacoustic Sensing of pH using a "Sonophore,", *The Analyst*. **2008**, *133*, 747 – 749.
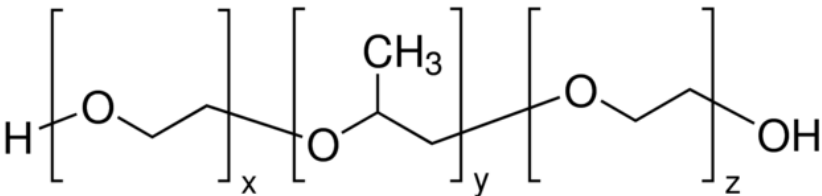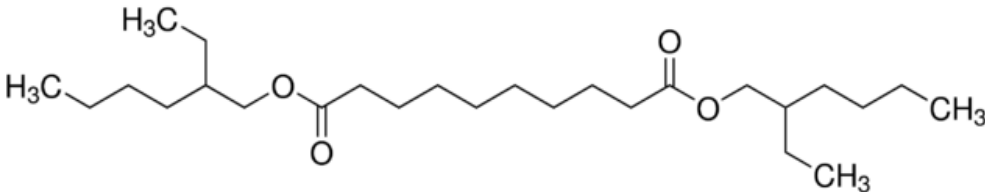
ACKNOWLEDGEMENT

The author acknowledges the University of Michigan Department of Chemistry for providing the fellowship, and the Kopelman group for technical support and data acquisition.

APPENDICES

A. Chemical structures of the major chemicals used in this study

Pluronic P123/F68

Bis (2-ethylhexyl)sebacate (DOS)

1, 6-Hexanediol dimethacrylate (HDMA)

Butyl methacrylate (BMA)

Figure A1. Chemical structures and abbreviations for the sodium sensor matrix, plasticizer, and

monomers.

Chromoionophore I (CHI1)

Sodium tetrakis[3,5-bis(trifluoromethyl)phenyl]borate (NaTFPB)
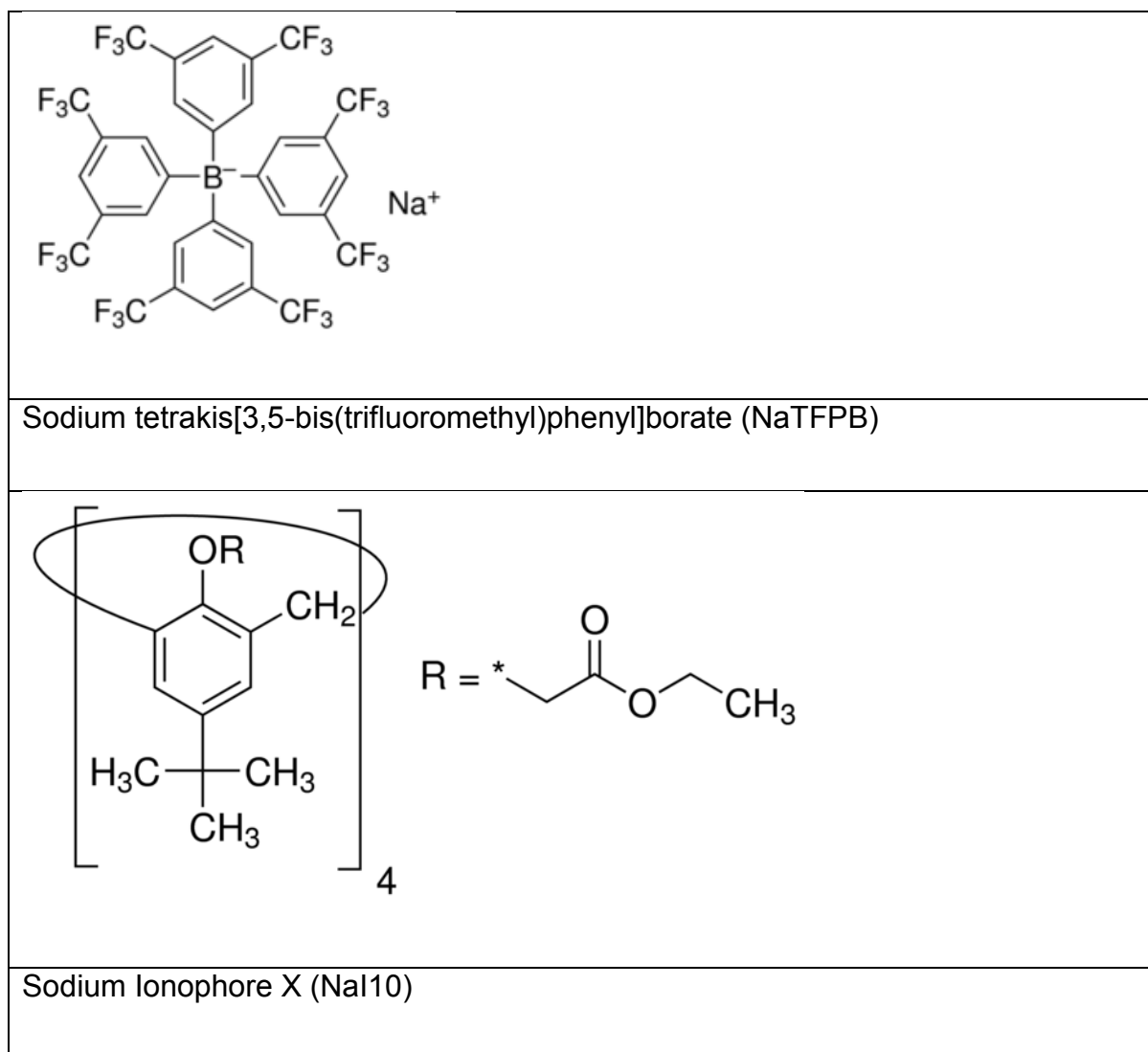

Sodium Ionophore X (NaI10)

Figure A2. Chemical structures and abbreviations for the sensing components of Na⁺ selective optode.

B. Calibration curves of absorption ratio vs. log(concentration) (mM)

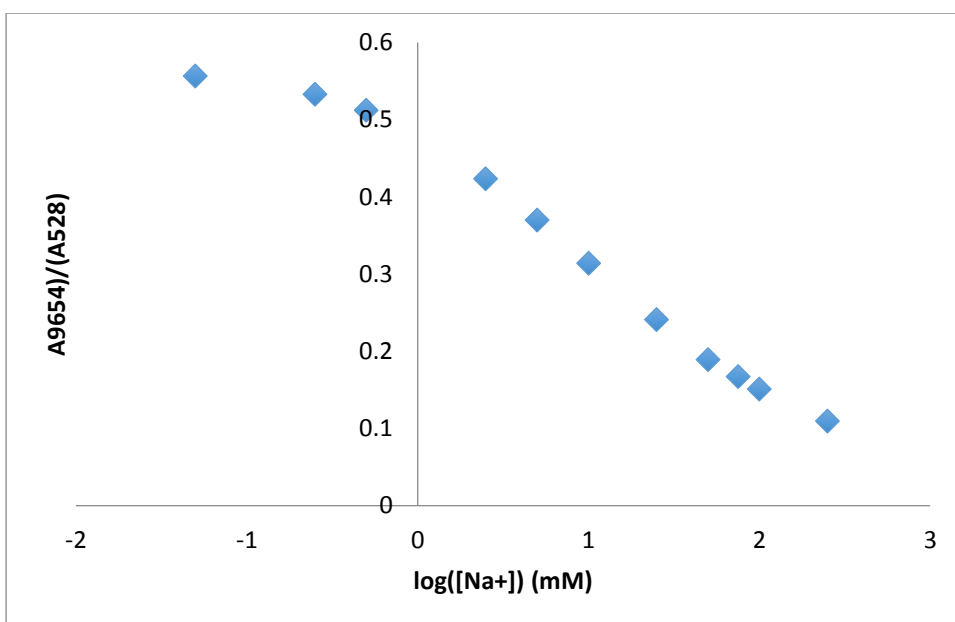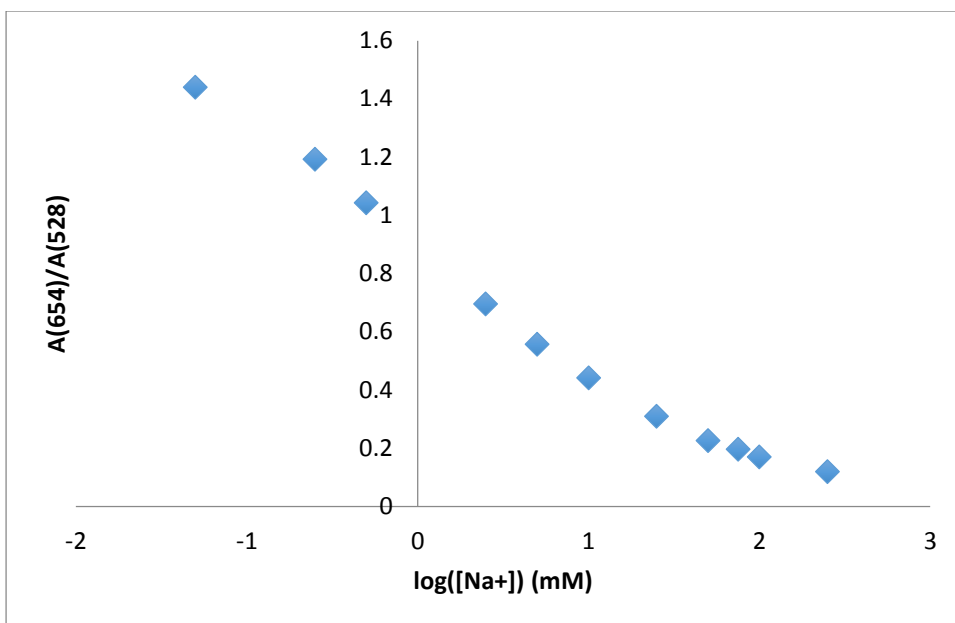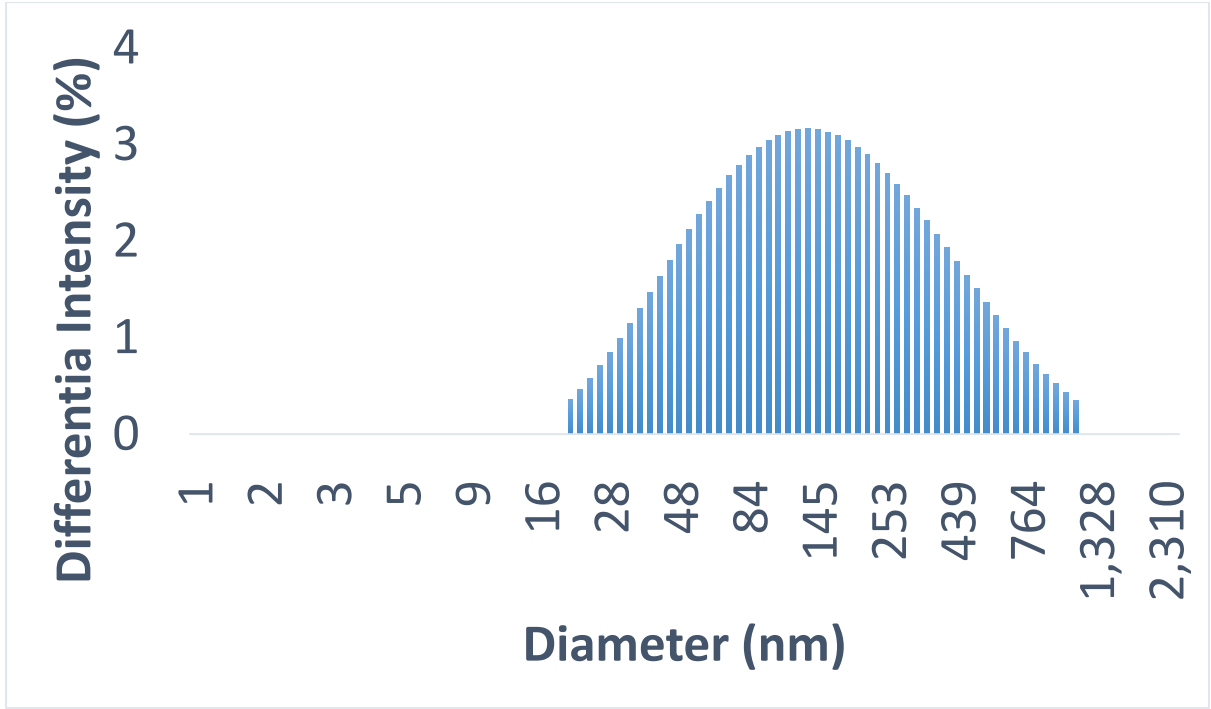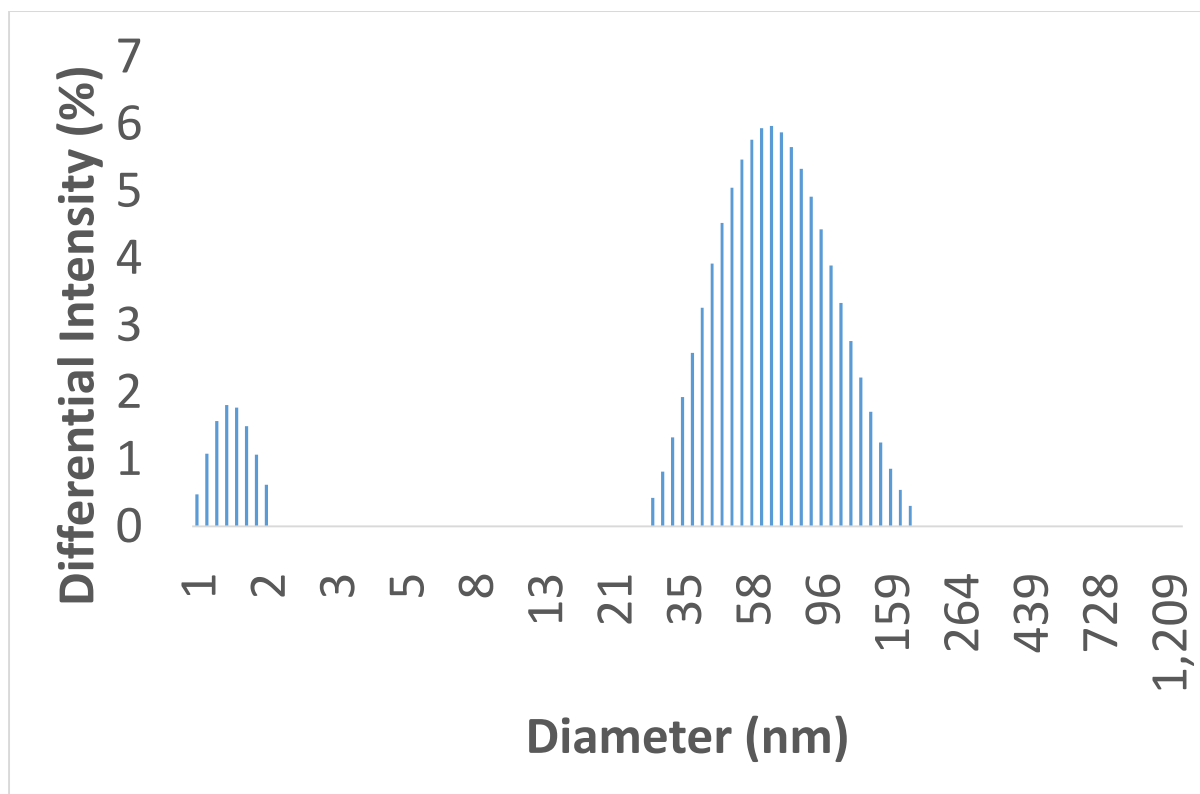Zoomed in of the Na⁺ calibration plots in potassium background of 4 and 100 mM.

Figure A3. Calibration curve of Na sensor response to Na⁺ in potassium background of 4 (up) and 100 mM (bottom).

C. Size distribution of the nanosensor pre and post-polymerization (from one
trial)

(a)

(b)

Figure A4. Size distribution of the nanosensor (a) before and (b) after radical polymerization. Data was collected by DLS from the preliminary study; not from any of the triplicate shown in this thesis.

Table A1. List of the average diameter, PDI, and zeta potential of the triplicate Na^+ nanosensors.

Sample #	1	2	3
Diameter (nm)	43.8±0.7	39.4±1.8	44.9±3.9
PDI	0.33±0.01	0.35±0.02	0.35±0.04
Zeta Potential (mV)	-78.2±2.7	-58.6±6.6	-39.1± 23.4 mV